ASTRONOMY & ASTROPHYSICS
SUPPLEMENT SERIES

JUNE 1987, PAGE 403

Astron. Astrophys. Suppl. Ser. **69**, 403-413 (1987)

Multifrequency radio continuum observations of extended galactic objects. II. Eleven objects from the 2695 MHz Effelsberg galactic plane survey

E. Fürst ([1]), T. Handa ([2]), W. Reich ([1]), P. Reich ([1]) and Y. Sofue ([2])

([1]) Max-Planck-Institut für Radioastronomie, Auf dem Hügel 69, D-5300 Bonn 1, F.R.G.
([2]) Nobeyama Radio Observatory (*), Tokyo Astronomical Observatory, University of Tokyo, Minamisaku, Nagano 384-13, Japan

Received July 10, accepted December 22, 1986

Summary. — The published 2695 MHz galactic plane survey with the Effelsberg 100-m telescope has been inspected for shell-type or complex objects, most of which have been formerly unidentified. Eleven objects have additionally been observed at 1420 MHz, 4750 MHz and 10.55 GHz. We also searched in the IRAS sky survey for associated infrared emission. Based on the available data, we propose the most probable identification of four new shell-type supernova remnants and seven HII regions. Among the HII regions we found a shell of about 30 × 22 pc in extent centred on a B0 star. Another thermal shell surrounds a slightly extended non-thermal source which might be a distant plerionic-type supernova remnant.

Key words : radio continuum emission — supernova remnants — HII regions.

1. Introduction.

This is the second of a series of papers presenting sensitive multifrequency radio continuum observations of extended galactic emission features. Most of these objects have been detected in the Effelsberg 2695 MHz galactic plane survey (HPBW= 4′.27), (Reich *et al.*, 1984). Supplementary radio data are provided by the galactic plane surveys at 1420 MHz (HPBW = 9′.3), (Reich *et al.*, 1987) with the 100-m telescope and at 10.55 GHz with the 45-m telescope (HPBW= 2′.7) of the Nobeyama Radio Observatory (Sofue *et al.*, 1984, 1987). Additional observations including linear polarization have been made at 4750 MHz with the 100-m telescope (HPBW = 2′.4). Based on the polarization and spectral index information the nature of many objects has been determined.

Nine objects have previously been reported by Reich *et al.* (1986, hereafter referred to as Paper I). The results for eleven more sources are presented here. The objects have been selected from the 2695 MHz survey according to shell-like morphology as being candidates for supernova remnants (SNRs). Some sources of complex structure have also been examined. Multifrequency observations with high angular resolution and including linear polarization measurements allow a decomposition and a correct classification of the different components.

Recently, Fürst *et al.* (1987) examined the far infrared emission in the IRAS all-sky survey (IRAS, 1985) associated with HII regions and SNRs. They found that SNRs of low surface brightness ($\Sigma_{1\,\mathrm{GHz}} < 3 \times 10^{-21}\,\mathrm{W\,m^{-2}\,Hz^{-1}\,sr^{-1}}$) generally do not show strong infrared emission : HII regions are in general bright and SNRs are dark in the infrared. This result can be used as a confirmation of the identification of sources based on their radio properties.

For all sources investigated in Paper I we searched for associated infrared emission. Objects which we identified as SNRs do not show up in the infrared, while the HII regions are bright. This result confirms our original identifications.

2. Observations.

The procedure of the observations at the various frequencies and their reduction has been described in paper I. For details the reader is referred to this paper.

(*) NRO, a branch of the Tokyo Astronomical Observatory, is a facility open for the general use by researchers in the field of astronomy and astrophysics.

Deviating from paper I, the centre frequency of the Nobeyama data is now 10.55 GHz.

As in paper I the flux density spectral index has been estimated from integrated flux densities as well as from differential spectral index plots (*TT*-plots) in order to investigate the influence of distortions by background emission. All relevant data of the individual sources are summarized in table I.

The linear polarization at 4750 MHz has been integrated and the average percentage polarization is included in table I.

Several discrete sources have been detected and are listed in table II.

3. Results.

In figures 1 to 11 we show contour plots (a) and integrated flux density spectra (b) of the sources. Maps are shown in main beam brightness temperature of total intensity (TP) at the highest available angular resolution, i.e. at 4750 MHz (HPBW= 2.'4). Additionally, polarized intensity (PI) has been plotted as bars in the E-field direction for sources with a positive detection. Maps at 1420 MHz, 2695 MHz and 10.55 GHz are included in the survey data and can be found in the papers by Reich *et al.* (1984, 1987) and by Sofue *et al.* (1984, 1987). Flux densities of small diameter sources are listed in table II. No flux densities at 1420 MHz are given because of generally high confusion and poor angular resolution at this frequency.

3.1 G18.2 − 0.3 ($\alpha_{50} = 18^h22^m.4$, $\delta_{50} = -13°15'$). — Figure 1(a) shows a complex of small diameter sources and extended emission. This object is associated with the HII region S53 (Sharpless, 1959). Six discrete sources have been separated (see Tab. II). Five of these are listed in the recombination line surveys by Wink *et al.* (1983) and/or Downes *et al.* (1980). The recombination line signal is relatively low for some of the sources and one source (at $l = 18°10'.7$, $b = -10'.1$) has not been detected. The aim of the present observation has been to obtain more information about these sources and to separate them from the underlying extended emission. Subsequently, the nature of this emission has been studied. The new flux density values of the small diameter sources are listed in table II. Subtracting these sources from the whole object leaves about 50 % of the total emission for the extended part: 11.0 Jy at 2695 MHz, 10.7 Jy at 4750 MHz, and 8.9 Jy at 10.55 GHz. These flux densities indicate a thermal nature of the diffuse emission. A size of 25 arcmin has been derived for the extended emission, larger than the 15 arcmin quoted by Dubout-Crillon (1976) for the corresponding HII region. The average distance to the small diameter sources is about 4.5 kpc according to the recombination line surveys by Wink *et al.* and Downes *et al.* (lower distance assumed). Adopting the same distance for the extended emission, we may estimate the relative masses contained in the small diameter sources and in the extended emission by using formulae given by Mezger and Henderson (1976). The total mass is of order 3300 $M_\odot$, 10 % of which is contained in the discrete sources. Size and electron number density of the extended emission are 32 pc and 10 cm^{-3}, respectively.

3.2 G21.1 − 0.35 ($\alpha_{50} = 18^h28^m.1$, $\delta_{50} = -10°43'$). — Two shell-type emission features are visible in the mapped area shown in figure 2(a). Both are associated with diffuse emission structures in the IRAS sky survey, but no emission was detected in the Palomar prints. Spectra of the northeastern shell A and the southwestern shell B are shown in figures 2(b) and 2(c) respectively. Both shells are most likely identified as HII regions. The cross in figure 2(a) marks the position of a B3 star (HD161568) of $m_v = 5.8$. The large off-centre position makes a physical relation of this star with any of the shells unlikely. We believe that the polarized emission in the central area of figure 2(a) is not related to the shells. Because the relative zero level was defined at the edge areas, some extended polarization features, as seen in the 2695 MHz polarization survey (Junkes *et al.*, 1987), likely influence the result. Observation of a larger field at 4750 MHz would be necessary to decide whether the polarized emission is associated with the shells.

3.3 G21.35 + 1.2 ($\alpha_{50} = 18^h23^m.0$, $\delta_{50} = -9°46'$). — This object (Fig. 3(a)) reveals a well-defined elliptical shell structure of $40' \times 30'$. The shell could not be separated from the 1420 MHz survey data because of the high confusing background, and is too weak to be seen in the 10.55 GHz survey. Faint emission has been found in the IRAS survey at 60 μ at the position of the southern part of the shell following the radio structure. In the Palomar prints faint shell-like emission related to the HII region CO31 (Dubout-Crillon, 1976) has been detected. These observations and the thermal radio spectral index make the identification of this shell as an HII region very likely.

The star HD142305 (marked in Fig. 3(a)) of spectral type B0 ($m_v = 8.4$) is located very close to the apparent centre of the shell. Could such a star excite the radio shell by its ultraviolet radiation ? According to formulae given by Mezger and Henderson (1976), the electron number density N_e of the shell is N_e (cm^{-3}) $\simeq 7/D^{1/2}$ (kpc), where D is the distance to G21.35 + 1.2. Here we have assumed an electron temperature of $T_e = 8000$ K. However, the distance to G21.35 + 1.2 is unknown. Unfortunately, the type of the B0 star (zero age main sequence, giant etc.) is also not known. For a zero age main sequence star ($M_v = -3.3$; Panagia, 1973) the distance would be $\lesssim 2.5$ kpc. In this case the excitation parameter U of G21.35 + 1.2 is U (pc cm^{-2}) < 35. This may be compared with $U = 17$ pc cm^{-2} calculated for

such stars (Panagia, 1973). Better optical information on this star is needed, however, to clarify this possible association.

3.4 G31.55 – 0.65 ($\alpha_{50} = 18^h48^m.6$, $\delta_{50} = -1°35'$). — This object is shown in figure 4(a) and consists of an elongated small diameter source (see Tab. II) with a flat radio spectrum located inside a shell structure of non-thermal emission. The polarization is less than 2 %. As seen in the Palomar prints, G31.55 – 0.65 is located at the southwest border of a strong emission region (HII region DU15, Dubout-Crillon, 1976). This thermal gas, if located in front of the source, may cause a strong depolarization. The radio spectral index estimation by different methods (see Tab. I) makes the identification of the shell as a SNR most likely. No emission is seen in the IRAS sky survey either at the position of the shell or at the flat spectrum source. A possible relation of both components is suggestive and would classify the entire object as a combined type SNR (Weiler, 1983). However, more observations are needed to settle that point.

3.5 G35.2 + 1.05 ($\alpha_{50} = 18^h49^m.3$, $\delta_{50} = 2°26'$). — The arc-like structure of G35.2 + 1.05 as shown in figure 5(a) is unusual for a galactic source. No related emission has been found in the Palomar prints, but G35.2 + 1.05 shows strong emission in the IRAS sky survey at 100 μ and 60 μ. Our spectral index determination (Tab. I) gives values between $\alpha = -0.14$ and $\alpha = -0.4$, slightly steeper than expected for an HII region. However, the strong infrared emission indicates that most of the emission from this area is thermal.

3.6 G36.6 – 0.7 ($\alpha_{50} = 18^h58^m.1$, $\delta_{50} = 2°52'$). — The area mapped (Fig. 6(a)) shows a complex emission structure. Most striking is the polarized feature in the southern part. There is a contamination of different sources in the northern area, which makes it impossible to determine the full extent of the polarized emission from the available data. The southern spur is not visible in the IRAS sky survey, while the small bent structure extending from $l = 36°38'$, $b = -35'$ in northern direction is visible. No optical emission has been found in the Palomar prints. Spectral index and polarization are a clear indication of the non-thermal nature. The average polarization percentage at 4750 MHz is about 15 %. A 6 % linear polarization has been found at 2695 MHz by Junkes (1986) with a large uncertainty due to baselevel problems. The available data suggest an identification as a SNR or part of it. A determination of the extent of the object in northern direction could not be made due to very high confusion with other sources. Consequently, no integrated flux densities could be given.

3.7 G36.75 – 0.15 ($\alpha_{50} = 18^h56^m.4$, $\delta_{50} = 3°16'$). — Figure 7(a) shows this unpolarized source, which is most likely identified as an HII region by its flat radio spectral index. No associated optical emission has been detected in the Palomar prints, but G36.75 – 0.15 is visible in the IRAS sky survey.

3.8 G39.5 + 0.55 ($\alpha_{50} = 18^h59^m.0$, $\delta_{50} = 6°01'$). — This source is shown in figure 8(a). The radio spectral index of $\alpha = -0.15$ suggests the identification as an HII region, although it is slightly polarized (3 ± 1 %). This polarization is concentrated in the outer areas of the source. We cannot exclude that the source contains both thermal and non-thermal emission. The sensitivity and angular resolution of the available data do not allow a separation of these components by using spectral index maps. More data would be necessary for clarification. No optical emission has been found in the Palomar prints, but G39.5 + 0.55 is located on a more extended ridge of infrared emission as visible in the IRAS sky survey.

3.9 G41.4 + 0.4 ($\alpha_{50} = 19^h03^m.1$, $\delta_{50} = 7°38'$). — Figure 9(a) shows the complex nature of this object. It is dominated by two small diameter sources and a shell-like feature. The slightly extended discrete source at $l = 41°25'.9$ and $b = 23'.5$, apparently located near the centre of the shell, is non-thermal with a linear polarization of 2.3 % at 4750 MHz (see Tab. II). Weak emission at 12 μ is listed in the IRAS point source catalogue. The nature of the source is unknown. In case it is galactic it has the characteristics of a plerionic-type SNR. The surface brightness ($\Sigma_{1\,\mathrm{GHz}} \simeq 2.0 \times 10^{-20}$ W m^{-2} Hz^{-1} sr^{-1}) suggests a distance of about 25 kpc (source size ~ 25 pc) according to the relations derived by Weiler and Panagia (1980). The large distance would explain the low degree of polarization. The source should be the subject of high angular resolution measurements. The other discrete source in the field at $l = 41°14'.0$, $b = 21'.7$ is much stronger and seems to be non-thermal as indicated by a decrease of its integrated flux density with frequency. However, a source of similar extent is seen in the IRAS sky survey. The eastern shell has a flat spectrum indicating its thermal nature. No emission has been found in the Palomar prints, but emission seen in the IRAS sky survey is associated. Whether there is a physical connection between one or both sources and the shell cannot be decided at present. The shell is most likely identified as an HII region.

3.10 G42.8 + 0.65 ($\alpha_{50} = 19^h04^m.9$, $\delta_{50} = 9°00'$). — This source (Fig. 10(a)) is identified as a shell-type SNR, too faint to be seen in the 10.55 GHz survey data. The estimated spectral index ($\alpha = -0.5$) is typical for this class of SNRs. The degree of polarization is about 22 % at 4750 MHz. The sensitivity of the available data at 2695 MHz is not sufficient to obtain an accurate value, but an upper limit of 10 % can be given. Additional polarization observations at higher frequencies are necessary to derive the magnetic field structure of this SNR. Associated optical or infrared emission has not

been found in either the Palomar prints or the IRAS sky survey.

3.11 G45.7 – 0.4 ($\alpha_{50} = 19^h14^m.1$, $\delta_{50} = 11°04'$). — A shell-type object is located near the centre of figure 11(a). As can be seen in the 2695 MHz survey data (Reich *et al.*, 1984) this shell is at the southeast border of an extended plateau of emission. It is also difficult to determine the true extent of the object in the northwest direction from the higher resolution 4750 MHz map shown here. No associated optical and infrared emission has been detected.

4. Summary.

From the eleven objects studied seven sources have been most likely identified as HII regions (G18.2 – 0.3, G21.1 – 0.35, G21.35 + 1.2, G35.2 + 1.05, G36.75 – 0.15, G39.55 + 0.55, G41.4 + 0.4). We cannot exclude the presence of some non-thermal emission in case of G21.1 – 0.35 and G39.55 + 0.55, because of some linearly polarized emission near the sources. One slightly extended source ($l, b = 41°25'.9, 23'.5$) shows the characteristics of plerionic-type SNRs. Four new supernova remnants have been identified (G31.55 – 0.65, G36.6 – 0.7, G42.8 – 0.65, G45.7 – 0.4).

A total of seven new supernova remnants have been found in paper I and in this paper. Some relevant parameters are presented in table III. The mean upper diameters D_R of the sources have been calculated from the upper envelope in the most recent $\Sigma - D$ diagram given by $\Sigma_{1\,GHz}$ [W Hz^{-1} m^{-2} sr^{-1}] = $2.51 \times 10^{-14} D_R^{-3.5}$ [pc] as compiled by Berkhuijsen (1986). The true diameters may be a factor of three smaller. We note that most of the newly detected SNRs have a lower surface brightness than the already known objects within the area of the 2695 MHz galactic plane survey. If there are yet undetected SNRs with high surface brightness they are likely to be found within the small diameter sources of the survey. The identification of these sources would require high resolution data, in addition to spectral and polarization information. Two objects of this type (G54.09 + 0.26 and G70.68 + 1.20) were recently identified as young SNRs by Reich *et al.* (1985).

Acknowledgements.

T. H. and Y. S. thank the Japanese Society for the Promotion of Sciences for a travel grant. P. R. is grateful to Prof. Akabane for financial support. We also thank Dr. M. Bird for critical reading of the manuscript. This work was done as part of the collaborative research program between NRO and MPIfR with financial support by the Japanese Society for the Promotion of Sciences and by the Alexander von Humboldt-Stiftung.

References

BERKHUIJSEN, E. M. : 1986, *Astron. Astrophys.*, in press.
DUBOUT-CRILLON, R. : 1976, *Astron. Astrophys. Suppl. Ser.* **25,** 25.
DOWNES, D., WILSON, T. L., BIEGING, J., WINK, J. E. : 1980, *Astron. Astrophys. Suppl. Ser.* **40,** 379.
FÜRST, E. *et al.* : 1987, in preparation.
IRAS Explanatory Supplement : 1985, C. A. Beichmann, G. Neugebauer, H. J. Habing, P. E. Clegg, T. J. Chester (Eds).
JUNKES, N. : 1986, Diploma Thesis, Bonn University.
JUNKES, N., FÜRST, E., REICH, W. : 1987, *Astron. Astrophys. Suppl. Ser.*, submitted.
MEZGER, P. G., HENDERSON, A. P. : 1976, *Astrophys. J.* **147,** 482.
PANAGIA, N. : 1973, *Astron. J.* **78,** 929.
REICH, W., FÜRST, E., STEFFEN, P., REIF, K., HASLAM, C. G. T. : 1984, *Astron. Astrophys. Suppl. Ser.* **58,** 197.
REICH, W., FÜRST, E., ALTENHOFF, W. J., REICH, P., JUNKES, N. : 1985, *Astron. Astrophys.* **151,** L10.
REICH, W., FÜRST, E., REICH, P., SOFUE, Y., HANDA, T. : 1986, *Astron. Astrophys.* **155,** 185.
REICH, W. *et al.* : 1987, in preparation.
SHARPLESS, S. : 1959, *Astrophys. J. Suppl. Ser.* **4,** 257.
SOFUE, Y., HIRABAYASHI, H., AKABANA, K., INOUE, M., HANDA, T., NAKAI, N. : 1984, *Publ. Astron. Soc. Jpn* **36,** 287.
SOFUE, Y. *et al.* : 1987, in preparation.
WEILER, K. W. : 1983, in « Supernova Remnants and their X-ray Emission », *IAU Symp.* No. **101,** J. Danziger and P. Gorenstein (Eds) (Reidel Publ. Co., Dordrecht) p. 299.
WEILER, K. W., PANAGIA, N. : 1980, *Astron. Astrophys.* **90,** 269.
WINK, J. E., WILSON, T. L., BIEGING, J. H. : 1983, *Astron. Astrophys.* **127,** 211.

TABLE I. — *General source parameters. Note : α_1 = spectral index from integrated flux density, $S_\nu \sim \nu^\alpha$. α_2 = spectral index from TT-plot 2695 MHz versus 4750 MHz, α_3 = spectral index from TT-plot 2695 MHz versus 10.55 GHz. Integrated flux density values include discrete sources except for marked cases.*

Source Name	Flux density (Jy) 1420 MHz	2695 MHz	4750 MHz	10.55 GHz	Polarization at 4750 MHz (%)	Flux density spectral index α_1	α_2	α_3	Most likely identification
G18.2-0.3	28.5±1.0	28.9±1.0	29.0±1.0	26.0±1.0	< 1	0.0	0.0	-0.1	HII
G21.1-0.35A	1.3±0.7	1.8±0.4	1.2±0.1	1.7±0.3	-	-	-0.13	-	HII
G21.1-0.35B	<0.5	0.38±0.05	0.35±0.05	0.39±0.1	-	0.0	-0.1	-	HII
G21.35+1.2	-	2.9±0.3	2.8±0.3	-	< 5	0.0	0.0	-	HII
G31.55-0.65	2.4±1.0	2.0±0.3	1.75±0.15	1.55±0.3	< 2	-0.2 (-0.4	-0.18 -0.25	-0.5 -0.8)[a]	HII+SNR
G35.2+1.05	11.4±1.6	7.4±0.6	6.4±0.7	4.9±0.9	< 2	-0.40	-0.14	-0.28	HII
G36.6-0.7	no integration possible				10 - 20[b]	-	-0.9[c]		SNR
G36.75-0.15	2.1±0.9	2.8±0.4	2.1±0.4	2.4±0.4	< 1	0.0	0.0	-0.2	HII
G39.55+0.55	2.8±0.4	2.4±0.2	2.3±0.1	2.0±0.5	3±1	-0.15	-0.15	-	HII?
G41.4+0.4	6.0±1.5	5.2±0.3	5.2±0.2	4.6±0.3	1±1	0.0[d]	-0.16[e]	-0.28[e]	Complex region with HII-shell
G42.8+0.65	2.4±0.6	2.0±0.2	1.5±0.2	-	22±9	-0.4	-0.6	-	SNR
G45.7-0.4	3.9±0.4[f]	3.2±0.3[f]	2.6±0.3[f]	2.2±0.3[f]	21±7	-0.3	-0.5	-	SNR

([a]) : southwestern shell.
([b]) : polarization of individual data points.
([c]) : southern part.
([d]) : after subtraction of the sources at l, b = 41°.234, 0°.362 and l, b = 41°.432, 0°.392.
([e]) : eastern shell.
([f]) : after subtraction of the source at l, b = 45°.828, − 0°.288.

TABLE II. — *List of small diameter sources.*

Galactic longitude (° ')	Galactic latitude (° ')	Right ascension α_{1950} (H M S)	Declination δ_{1950} (° ' ")	Flux density 2695 MHz	4750 MHz	10.55 GHz	IRAS point source	Comments S ~ $\nu^{-\alpha}$	Size (arcmin)
18 08.5	-0 17.9	18 22 14	-13 18 03	5.3 ±0.5	5.5 ±0.2	5.3 ±0.3	+	α = 0.0	1.4±0.05
18 10.7	-0 10.1	18 21 50	-13 12 26	-	1.7 ±0.2	2.3 ±1.1	+		3.4±0.2
18 11.0	-0 24.5	18 22 43	-13 18 58	1.9 ±0.3	2.8 ±0.2	2.3 ±0.4	+		2.9±0.1
18 13.1	-0 15.0	18 22 13	-13 12 37	-	3.5 ±0.4	2.8 ±0.5	-		4.3±0.3
18 15.5	-0 18.8	18 22 31	-13 12 14	3.1 ±0.7	3.4 ±0.4	3.1 ±0.4	+	α = 0.0	2.9±0.2
18 18.1	-0 24.1	18 22 55	-13 12 30	1.2 ±0.3	1.4 ±0.1	1.3 ±0.2	+	α = 0.0	pl
21 06.9	1 25.2	18 21 47	- 9 52 06	-	0.07±0.01	-	-		0.9±0.3
21 10.7	1 30.4	18 21 35	- 9 46 15	-	0.05±0.01	-	-		pl
21 26.8	1 32.6	18 21 58	- 9 31 06	-	0.05±0.02	-	-		1.7±0.6
21 36.4	0 56.3	18 24 27	- 9 39 40	0.25±0.06	0.08±0.01	-	-		pl
31 39.1	-0 39.7	18 48 52	- 1 30 05	0.53±0.2	0.72±0.05	0.77±0.2	-		(6.4±0.2)x (2.5±0.1)
36 31.1	-0 58.0	18 58 55	2 40 42	-	0.05±0.01	-	+		pl
36 41.9	-0 37.9	18 58 04	2 59 33	-	0.18±0.02	-	-		pl
39 34.8	0 24.7	18 59 41	6 01 46	-	0.10±0.02	0.11±0.07	-		1.9±0.3
41 14.0	0 21.7	19 02 57	7 28 22	1.05±0.05	0.87±0.05	0.68±0.34	-		2.4±0.1
41 21.0	0 31.8	19 02 34	7 39 12	-	0.05±0.02	-	+		pl
41 25.9	0 23.5	19 03 13	7 39 44	0.81±0.08	0.65±0.05	0.54±0.19	+	2.3% pol. at 4750 MHz α = 0.3	(3.5±0.2)x (2.3±0.2)
42 53.6	0 34.4	19 05 18	9 02 28	0.34±0.03	0.30±0.01	-	-		pl
45 29.0	-0 30.1	19 14 04	10 49 41	-	0.04±0.02	-	-		1.5±1.5
45 41.2	-0 13.8	19 13 29	11 08 09	0.15±0.04	0.17±0.03	-	+		1.7±0.3
45 49.7	-0 17.3	19 13 58	11 13 59	0.69±0.07	0.78±0.04	-	+		1.0±0.1
45 52.5	-0 36.6	19 15 13	11 07 23	-	0.05±0.01	-	-		pl
45 56.6	-0 24.1	19 14 35	11 16 47	-	0.14±0.02	-	+		1.0±0.5

pl = point like source

TABLE III. — *Parameters of newly found supernova remnants.*

Name	S (1GHz) (Jy)	Size (arcmin)	Σ_{1GHz} (Watt m^{-1} Hz^{-1} sr^{-})	D_R (pc)
G16.85-1.05	4.9	30 x 24	1.0×10^{-21}	< 130
G30.7+1.0	5.0	24 x 18	1.7×10^{-21}	< 110
G31.55-0.65	1.5	18	7.0×10^{-22}	< 140
G36.6-0.7	?	> 25	?	?
G42.8+0.65	2.0	24	5.2×10^{-22}	< 150
G45.7-0.4	3.8	22	1.2×10^{-21}	< 120
G73.9+0.9	9	22	2.8×10^{-21}	< 95

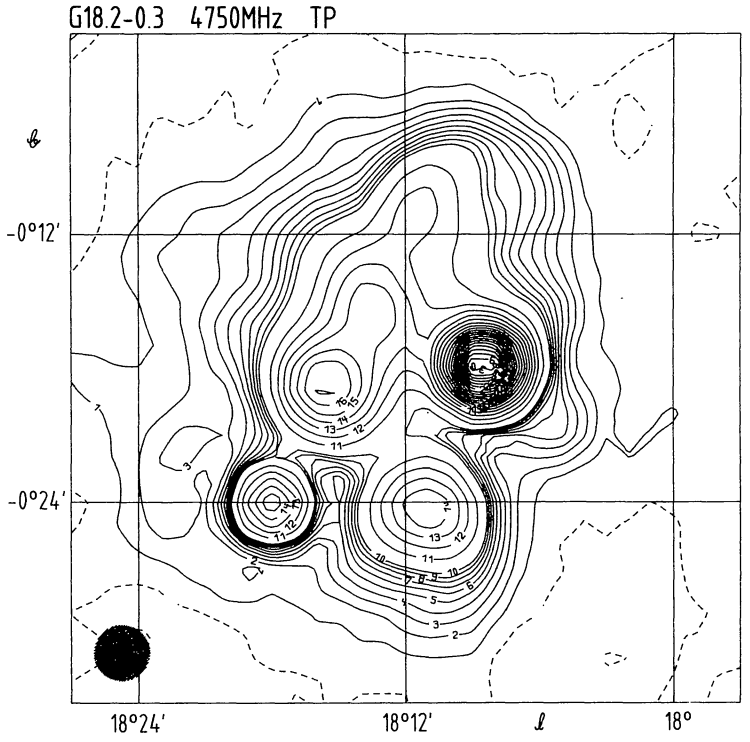

(a)

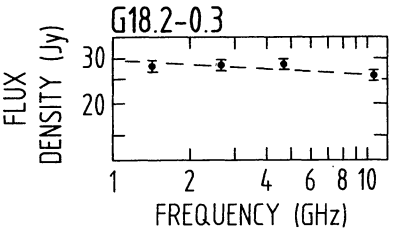

(b)

FIGURE 1. — Contour plot (a) and spectrum (b) of G18.2 – 0.3. Contour steps are in 100 mK T_B up to 1 K T_B and further in 500 mK T_B. The HPBW is 2.'4, as indicated in the lower left corner. The r.m.s. noise is 20 mK T_B.

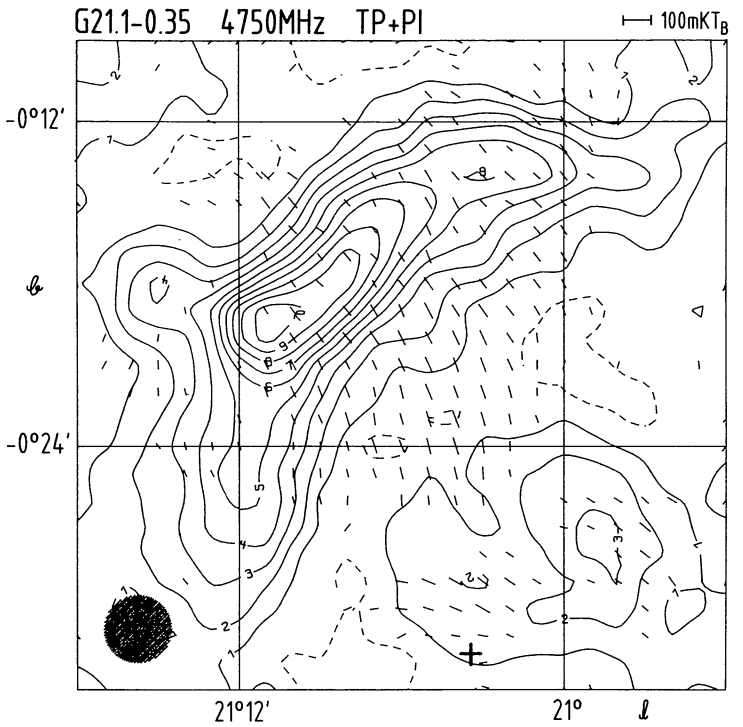

(a)

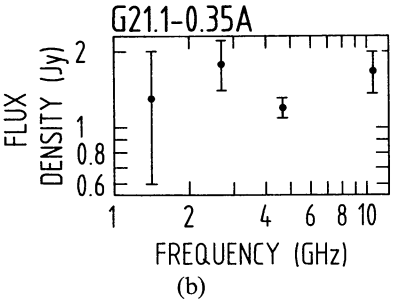

(b)

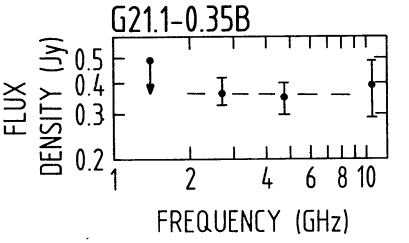

(c)

FIGURE 2. — Contour plot (a) and spectrum (b) of G21.1 – 0.35. Contour steps are in 50 mK T_B. The r.m.s. noise is about 20 mK T_B in TP and 11 mK T_B in PI. PI is shown above 25 mK T_B. The cross denotes the B3 star HD161568. The integrated spectrum of the northern arc is shown in figure 2(b) and that of the source southwest in figure 2(c).

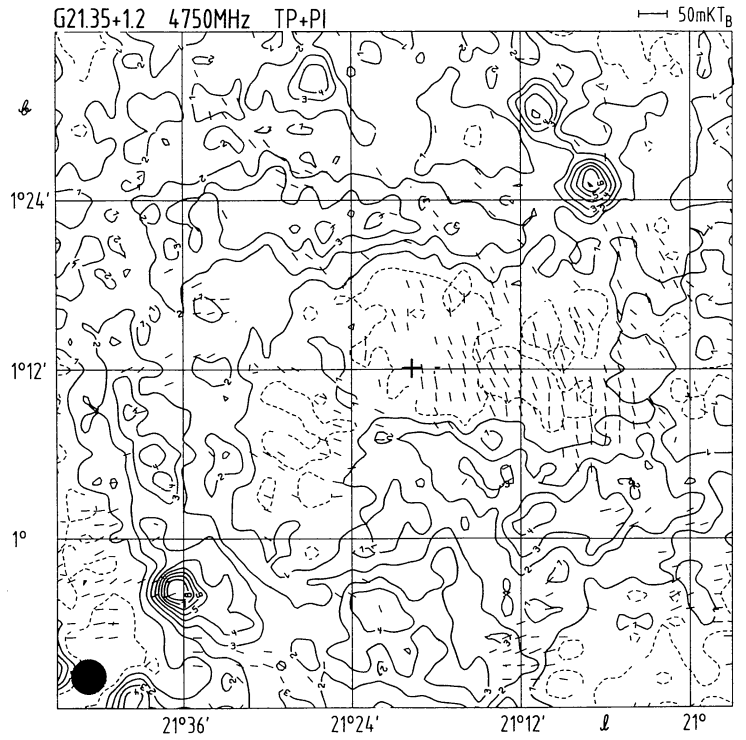

(a)

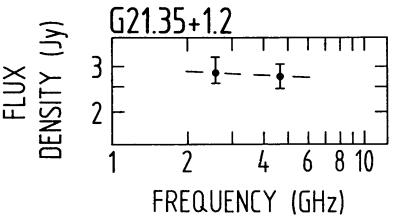

(b)

FIGURE 3. — Contour plot (a) and spectrum (b) of G21.35 + 1.2. Contour steps are in 25 mK T_B. The r.m.s. noise is about 15 mK T_B in TP and 11 mK T_B in PI. PI is plotted above 25 mK T_B. The cross denotes the B0 star HD142305.

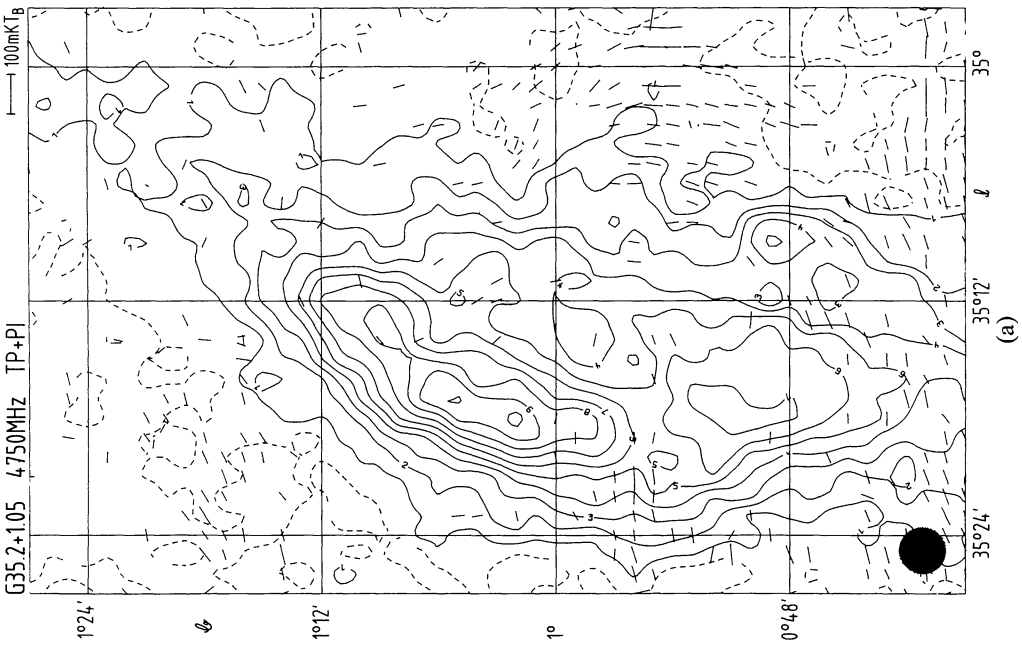

FIGURE 5. — Contour plot (a) and spectrum (b) of G35.2 + 1.05. Contour steps are in 40 mK T_B. The r.m.s. noise is about 20 mK T_B in TP and 12 mK T_B in PI. PI is plotted above 25 mK T_B.

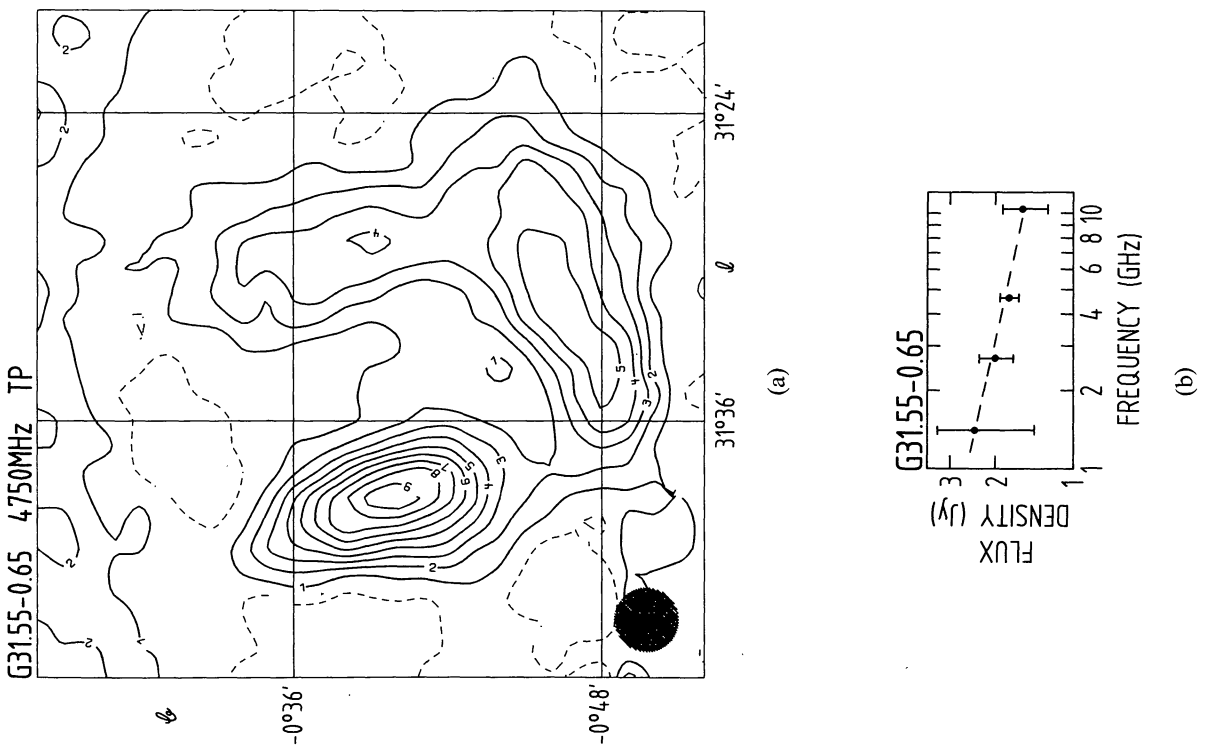

FIGURE 4. — Contour plot (a) and spectrum (b) of G31.55 – 0.65. Contour steps are in 50 mK T_B. The r.m.s. noise is about 25 mK T_B.

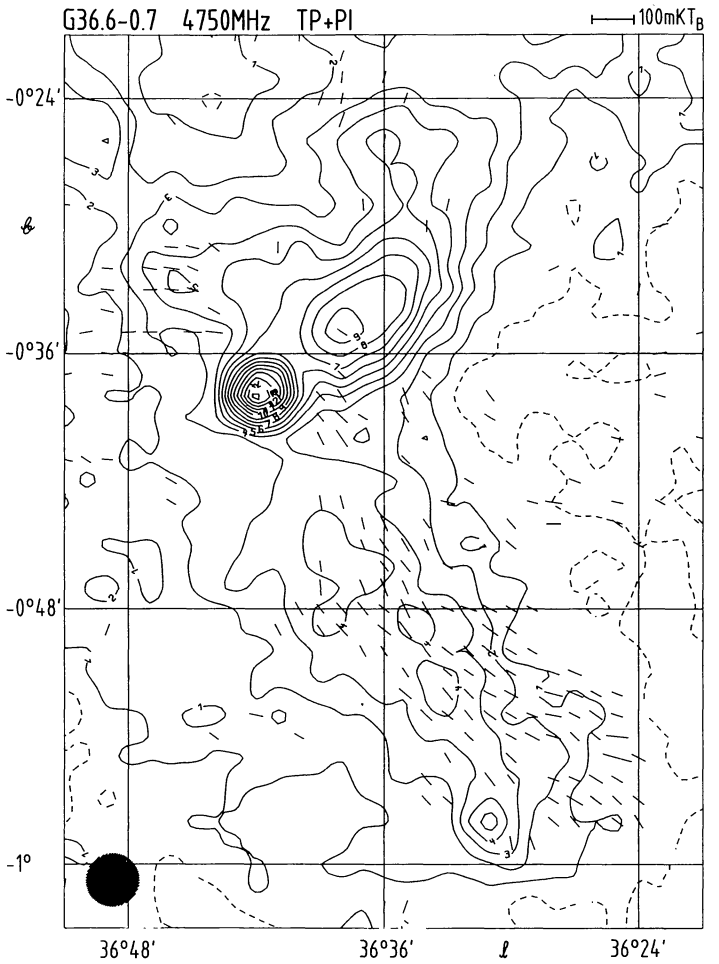

FIGURE 6. — Contour plot (a) of G36.6 – 0.7. Contour steps are in 40 mK T_B. The r.m.s. noise is about 15 mK T_B in TP and 11 mK T_B in PI. PI is plotted above 25 mK T_B.

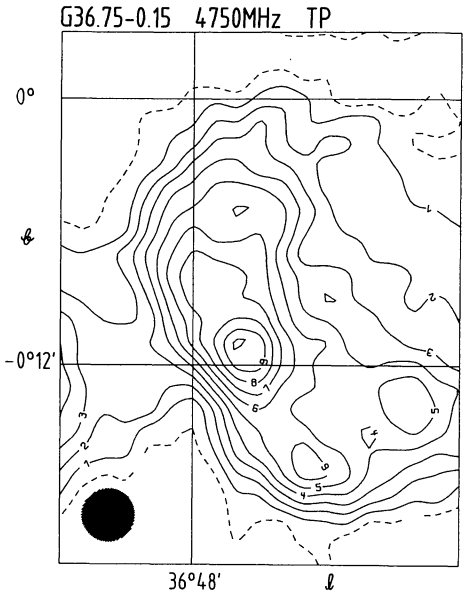

(a)

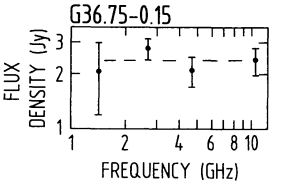

(b)

FIGURE 7. — Contour plot (a) and spectrum (b) of G36.75 – 0.15. Contour steps are in 40 mK T_B. The r.m.s. noise is about 20 mK T_B.

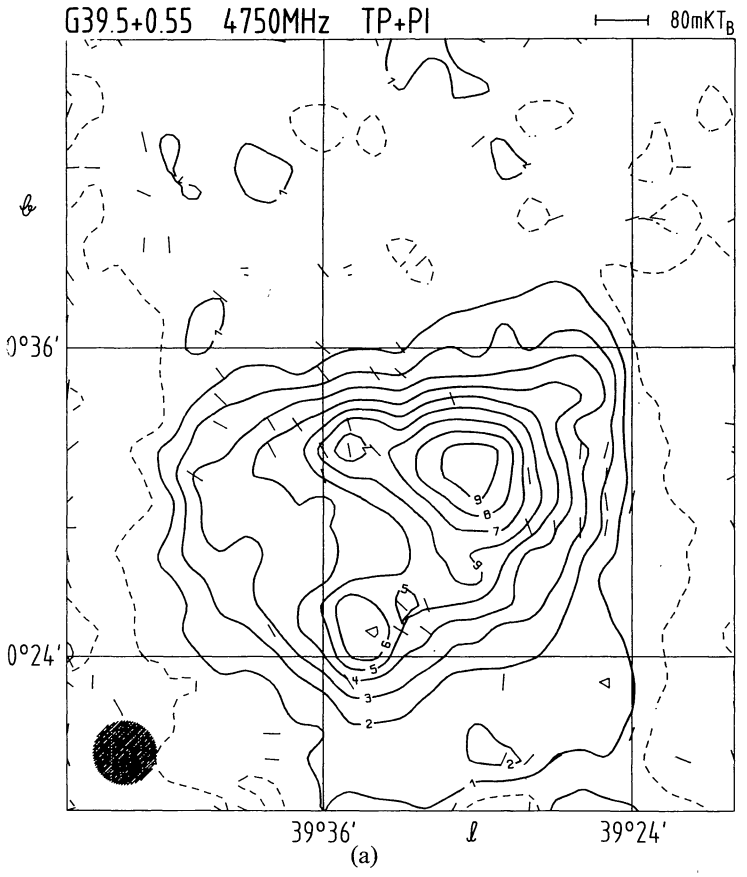

(a)

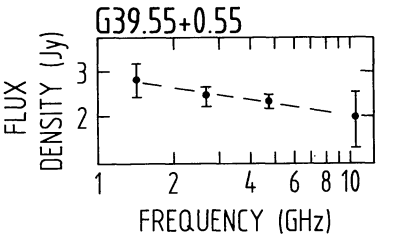

(b)

FIGURE 8. — Contour plot (a) and spectrum (b) of G39.5 + 0.55. Contour steps are in 40 mK T_B. The r.m.s. noise is about 16 mK T_B in TP and 11 mK T_B in PI. PI is plotted above 20 mK T_B.

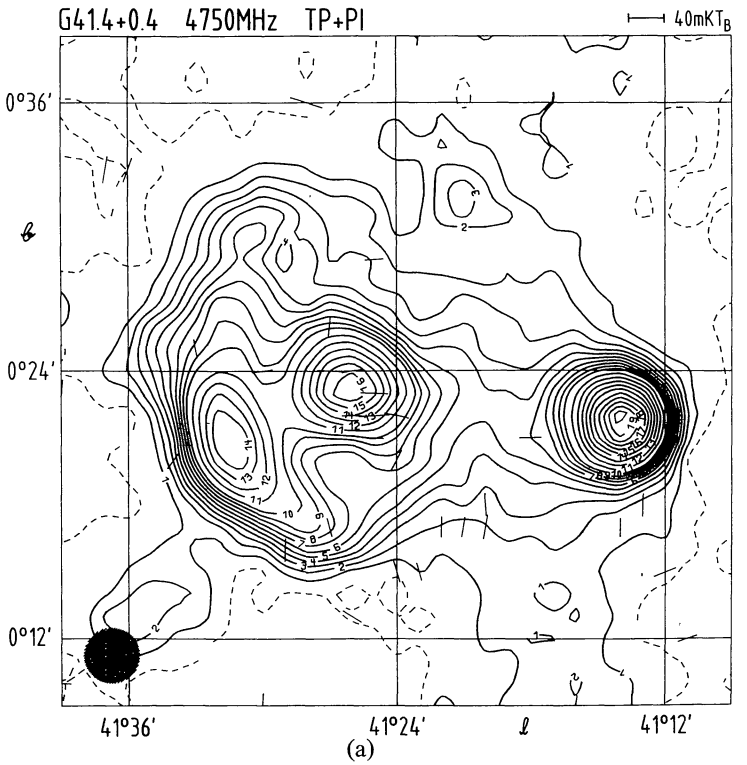

(a)

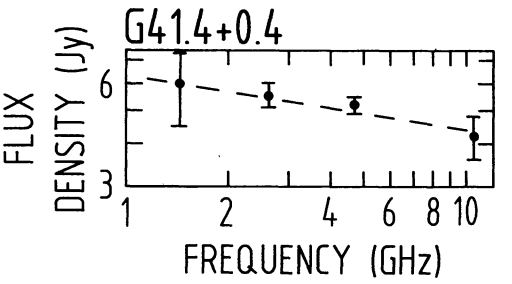

(b)

FIGURE 9. — Contour plot (a) and spectrum (b) of G41.4 + 0.4. Contour steps are in 40 mK T_B up to 400 mK T_B and further in 80 mK T_B. The r.m.s. noise is about 15 mK T_B in TP and 10 mK T_B in PI. PI is plotted above 20 mK T_B.

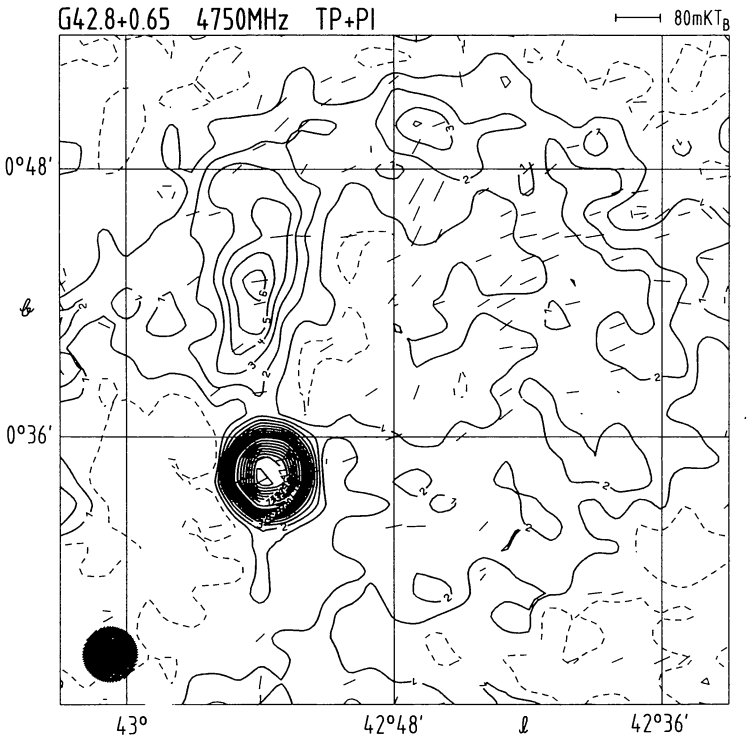

(a)

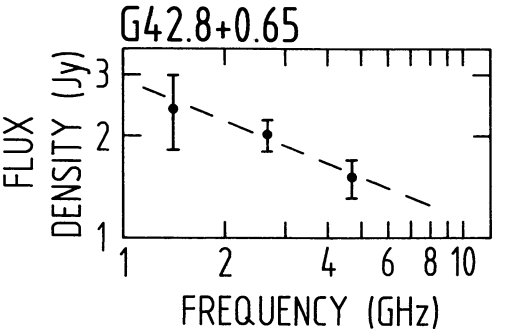

(b)

FIGURE 10. — Contour plot (a) and spectrum (b) of G42.8 + 0.65. Contour steps are in 25 mK T_B up to 250 mK T_B and further in 50 mK T_B. The r.m.s. noise is about 15 mK T_B in TP and 10 mK T_B in PI. PI is plotted above 20 mK T_B.

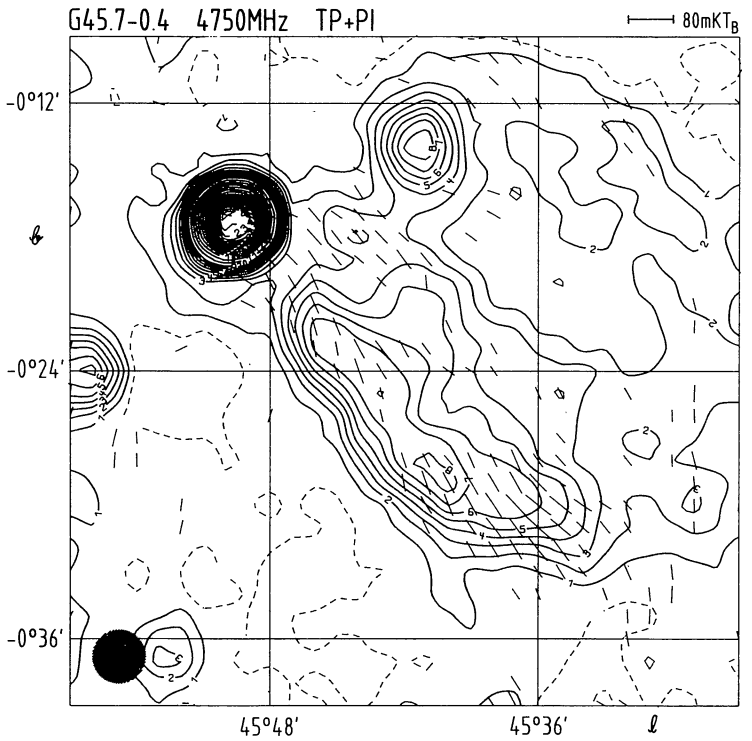

(a)

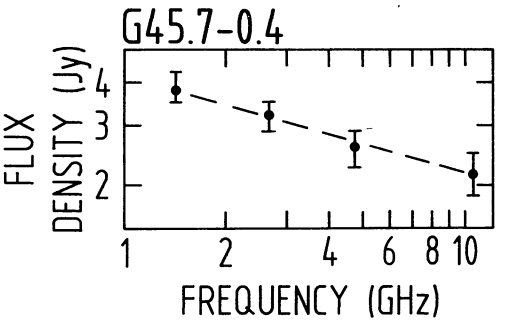

(b)

FIGURE 11. — Contour plot (a) and spectrum (b) of G45.7 – 0.4. Contour steps are in 40 mK T_B up to 400 mK T_B and further in 80 mK T_B. The r.m.s. noise is about 13 mK T_B in TP and 9 mK T_B in PI. PI is plotted above 20 mK T_B.